Journal of Sedimentary Research

Journal of Sedimentary Research, 2017, v. 87, 1–11
Research Methods
DOI: http://dx.doi.org/10.2110/jsr.2016.92

DISTINGUISHING DEPOSITIONAL SETTING FOR SANDY DEPOSITS IN COASTAL LANDSCAPES USING GRAIN SHAPE

JORDAN BLAIR REGLIN EAMER,*[1,2] DAN HIRSH SHUGAR,[†,1,2] IAN JAMES WALKER,[‡,1,2] OLAV B. LIAN,[1,3] AND CHRISTINA M. NEUDORF[1,3]

[1]*Hakai Institute, Heriot Bay, British Columbia V0P 1H0, Canada*
[2]*Coastal Erosion and Dune Dynamics Laboratory, Department of Geography, University of Victoria, Victoria, British Columbia V8W 2Y2, Canada*
[3]*Department of Geography and the Environment, University of Fraser Valley, 33844 King Road, Abbotsford, British Columbia, Canada*
e-mail: ianjwalker@asu.edu

ABSTRACT: **Several methods exist that use sediment properties to characterize depositional setting and related mechanisms of transport, including analysis of grain-size distributions, sediment petrology, micromorphology, and grain structure. Techniques that rely on electron or optical microscopy produce results with varying degrees of success and applicability. Here, a new method is presented and used to differentiate between littoral and eolian sands that were extracted from recently formed landforms, as well as landforms that are from mid to late Holocene in age. The method utilizes a standard optical microscope with a mounted digital camera, paired with freely available software (ImageJ) to characterize grain shape parameters. The method was tested on nearly 6000 sand grains from samples with varied transport histories, and it was found that grain solidity was the most distinguishable characteristic between eolian and littoral samples, differentiating them 86% of the time for calibration samples. The method was used to correctly identify the mechanism of transport for 76% of the samples. Patterns in the results indicated that this method could be extended to link potential sediment sources to various depositional basins, and future work includes testing the method in areas with a different mineralogy and/or landscape history.**

INTRODUCTION

Differentiation of beach and coastal dune environments in the Quaternary record is important for environmental reconstructions and interpreting changes in relative sea-level. For example, estimating the elevation difference between a coastal foredune and the intertidal beach helps refine the indicative meaning, or relationship of a sample to tidal range, of those landforms (Shennan et al. 2006). Efforts to characterize depositional setting based on sediment characteristics have included scrutiny of traditional grain-size distributions (GSD) (e.g., Mason and Folk 1958; Friedman 1961; Folk 1966; Rogerson and Hudson 1983; Sun et al. 2002; Shugar and Clague 2011; Purkait and Majumdar 2014), analyses of sediment petrology (e.g., Potter 1986; Kasper-Zubillaga and Dickinson 2001), examination of grain micromorphology as seen in thin section (e.g., Lewis et al. 2010; van der Meer and Menzies 2011; Bendle et al. 2015; Neudorf et al. 2015a), and analyses of grain structure parameters derived from electron microscopy (e.g., Krinsley and Donahue 1968; Clague 1976; Culver et al. 1983; Mazzullo et al. 1986; Vos et al. 2014), or simple optical microscopy (e.g., Fournier 1964; Soutendam 1967; Warnke and Gram 1969; Moss and Green 1975).

The contrast in sand transport processes is significant between coastal dunes (dominated by eolian processes) and intertidal beaches (controlled by littoral processes). This is largely due to the transport medium, with water providing more buoyancy force which reduces the downward gravitational force and grain momentum when compared to wind. This results in less impact force when water-entrained grains impact the bed, and also a higher impact threshold for maintaining grain entrainment. This leads to detectable differences in both the size distribution and shape of sand grains contained in these respective deposits. Generally, GSDs of littoral sands are negatively skewed or symmetric, while those of eolian sands are more positively skewed (Mason and Folk 1958; Friedman 1961). Although this general tendency does not hold true everywhere (e.g., Friedman 1961; Rogerson and Hudson 1983; Purkait and Majumdar 2014), the application of more advanced statistics has resulted in greater success in discerning the mechanism of transport (e.g., Vincent 1986; Purkait 2010). In addition, surface microstructures on sand grains, to the extent where grain roundness is affected, can be used to indicate longshore transport (e.g., Kasper-Zubillaga et al. 2005) or, importantly for this study, eolian transport processes. This can be attributed to a number of processes, including preferential chemical weathering of eolian sediments (Kasper-Zubillaga et al. 2005) or because wind preferentially entrains spherical and rounded sand grains. On the latter, particle shape has implications for the internal angle of friction in coastal sediments (Stark et al. 2014), and can affect grain packing, the point of initiation and the rate of eolian sediment

* Present Address: Applied Geospatial Lab, Department of Geography, University of Calgary, 2500 University Drive NW, Calgary Alberta T2N 1N4, Canada
† Present Address: Water, Sediment, Hazards, and Earth-surface Dynamics (waterSHED) Laboratory, School of Interdisciplinary Arts and Sciences, University of Washington, Tacoma, Washington 98402, U.S.A.
‡ Present Address: School of Geographical Sciences and Urban Planning, School of Earth and Space Exploration, Arizona State University, 975 South Myrtle Avenue, Tempe, Arizona 85281, U.S.A.

Published Online: January 2017
Copyright © 2017, SEPM (Society for Sedimentary Geology) 1527-1404/17/087-001/$03.00

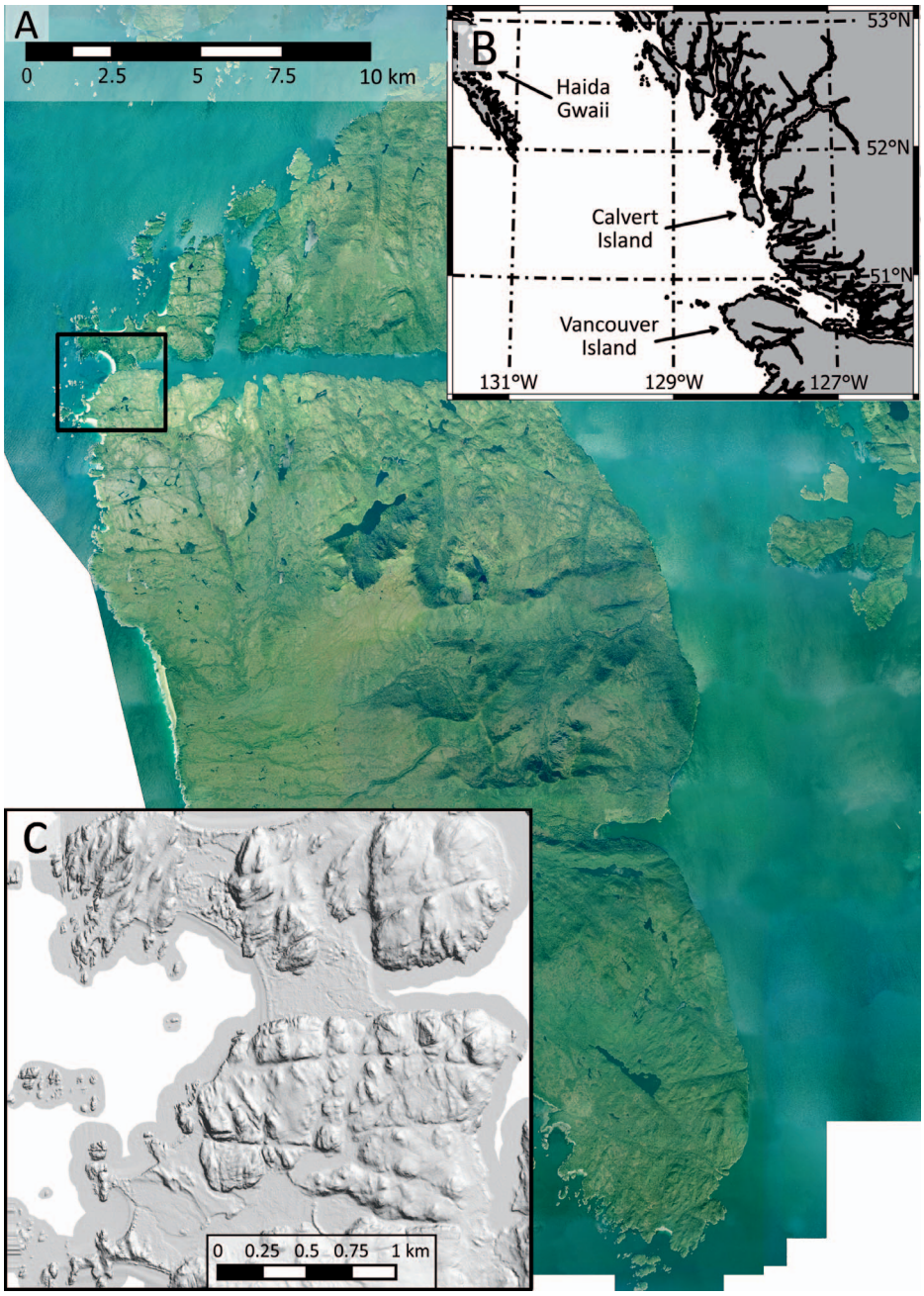

FIG. 1.—**A)** Digital orthophoto of Calvert Island, on the central coast of British Columbia. Box shows the location of the study area, shown in Part C. **B)** Inset map in upper right shows the location of the study area on the Pacific coast of British Columbia. **C)** Inset map showing the 2 m hillshaded lidar DEM for the study area. The lidar data were obtained and processed by Rob Vogt of the UNBC lidar Research Group, Derek Heathfield of the Hakai Institute Coastal Sandy Ecosystem Program, and Dan Shugar and Jordan Eamer of the Coastal Erosion and Dune Dynamics laboratory.

transport (Anderson et al. 1991). Thus, eolian sediment transport on a beach results in shape sorting, where a deflation lag with high proportions of irregular and angular grains remains, and an increasing concentration of spherical and rounded sand grains occurs several meters downwind of the beach surface (Mazzullo et al. 1986).

In this study, two-dimensional shape parameters of individual grains were investigated to test the hypothesis that sand grains associated with eolian transport could be differentiated from those associated with littoral transport using this method alone. The main objective of this study was to develop a method that required minimal equipment, freely available software, and a user-friendly methodology. The resulting method involved a standard binocular optical microscope with digital camera and the freely distributed image-analysis software, ImageJ (Rasband 2010). The method is described and evaluated using samples from modern and relict (Holocene age) beach and dune systems found on Calvert Island on the central coast of British Columbia, Canada.

STUDY AREA

Calvert Island is located on the central coast of British Columbia in Queen Charlotte Sound, about 70 km northwest of Vancouver Island and about 200 km southeast of Haida Gwaii (Fig. 1). The bedrock is composed mainly of Early Cretaceous tonalite, quartz diorite, granite, granodiorite, and diorite of the Calvert Island Pluton with diorite-dominated rocks of unknown age cropping out mostly in the central, eastern, and southeastern parts of island (Roddick 1996). Exposed glacial sediments on Calvert Island are largely confined to its western half, with inland areas otherwise absent of much surficial cover, particularly in the northwest. Small areas of glaciofluvial outwash have been mapped in the northwest part of the island.

Raised (relict) shorelines also exist, and it is believed that relative sea level has fluctuated less than a few meters since the late Pleistocene (McLaren et al. 2014), which is markedly different from other neighboring regions on the Pacific coast of North America (Shugar et al. 2014). The west-facing coastline is predominantly bedrock except in the northwest, where cobbly and sandy embayed beaches with localized dunes, tombolos, and spits (Fig. 1) occur. The northwestern portion of Calvert Island contains a high proportion of the mid to late Holocene accretionary sediments. Their geochronology suggests a complex landscape history that is difficult to interpret based on landform associations alone (Neudorf et al. 2015b).

METHODOLOGY

The method developed for this study involves the following five stages: (1) samples were collected from a variety of modern, active beach and dune settings to form a calibration dataset; (2) calibration samples collected in the first step were mechanically sieved into 1/4 φ Wentworth size classes and subsampled in each size class with a sufficient sample size; (3) suCsamples of several hundred grains from each size class were imaged and shape parameters were calculated using the ImageJ software; (4) the size class and shape parameters that show the largest statistical difference between littoral and eolian sands were selected by difference of mean statistical tests; and (5) using the ideal size class and shape parameters, the calibration samples were compared to additional samples to determine the mechanism of transport (MoT). Each step is described in detail below.

Sample Collection

Samples used in this study included a range of modern and mid to late Holocene shovel test and core samples (Fig. 2) collected from diagnostically distinct landforms. Modern sand samples were collected to approximately 10 cm depth from the surface, and relict sand samples were collected below modern soils, from the parent material (C horizon) wherever possible.

For method development, lower- and upper-littoral-zone samples were collected from both West and North beaches (samples L1, L2, L3, and L4, Fig. 2) to provide calibration samples and to represent potential source sediments for eolian transport into the region between the beaches. The lower beach (intertidal) samples were taken just above low tide and represent sediments deposited on the foreshore by littoral processes. The upper beach (backshore) samples were collected approximately one meter seaward from incipient dunes, so as to best represent a beach sediment still dominated by littoral processes, yet influenced partly by eolian transport. It is recognized that the processes of sediment transport at the beach–dune interface are complex and, thus, sediment properties in this zone are expected to be highly variable spatially and temporally (Houser 2009). However, the sampling methodology, where a depth-integrated sample was taken in areas with clear eolian influence (edge of incipient dunes), should allow some confidence that upper-beach samples include some eolian and some littoral sand. Modern dune samples collected for calibration were collected from the established foredune crest (sample A1), an unvegetated deflation basin in a blowout dune (sample A2), and a vegetated depositional lobe of a blowout (sample A3), with landform morphology indicating potential landward eolian sediment transport from the positions of sample A1 to A2, and A2 to A3. It is important to note that this portion of the landscape was much more active and connected, with respect to eolian activity, as recently as the late 1990s. For the calibration dataset, this progression on West beach (L1 to A3) represents a cross-shore profile to show decoupling of shape-sorted grains from swash to dune and farther landward.

Samples from other geologic studies performed in the area, specifically a late Pleistocene landscape reconstruction, were used to develop and validate the method described here. Ancillary data, including soil properties, fossils, stratigraphy, landform geomorphology, and geochronology have allowed interpretation of the MoT. Samples include modern dune and beach samples (S1 and S10, respectively), relict dune complex samples (S2, S3, S4, S5, S8), relict foredune samples (S6, S7, S11, S12), and one relict beach sample (S9) (Fig. 2). These samples were collected in conjunction with sampling for optical dating in a related study (Neudorf et al. 2015b). Between 200 and 400 g were collected for these samples at depths ranging from 20 to 60 cm below the ground surface, depending on the amount of soil development and the depth of the C horizon. All samples have associated ages determined from optical dating and are mid-Holocene (4.20 ± 0.33 ka) to modern (0.032 ± 0.005 a) in age (Neudorf et al. 2015b), thus providing a good temporal range of samples from which to develop and test the method.

Five samples were also collected from two percussion cores (C1 and C3) obtained in a lake basin between West and North beaches that is partially divided by a ridge of vegetated unconsolidated sand (interpreted as a foredune) and bedrock (Fig. 2). The samples were collected from distinct sand beds at depths of 49, 62, and 95 cm (samples C1-49, C1-62, and C1-95) in core 1, and 20, and 40 cm (samples C3-20 and C3-40) in core 3. The sand beds are separated by organic material, and some of this was used for accelerator mass spectroscopy radiocarbon dating, and have ages that date to the late Holocene, with basal ages of 1700–1820 cal yr BP. One sample of well-sorted eolian sand that yielded an optical age of 645 ± 64 cal yr BP (Neudorf et al. 2015b) was collected from a vibracore sample from the foredune ridge in the lake.

GSD and Subsampling

For all samples, except those collected from cores (due to insufficient mass), GSDs were obtained by mechanical sieving using WS Tyler test sieves stacked at 1/4 φ intervals. For each sample, 200 g of sediment was dried in a laboratory oven for 24 hr at 105°C and subsequently mechanically split. Samples were sieved in a Ro-Tap sieve shaker for 15 minutes and each sieve fraction was weighed with an electronic balance. Textural parameters (mean, sorting, skewness, and kurtosis) were calculated graphically using the Folk and Ward (1957) method and GRADISTAT Version 8 (Blott and Pye 2001). In addition, one-way analysis of variance (ANOVA) statistical tests were performed on each textural parameter separated into eolian and littoral sample groups. For example, one of the four hypothesis tests was as follows: H_0: The two sample groups (eolian or littoral) of mean grain-size are drawn from the same population; H_1: The two sample groups of mean grain-size are drawn from different populations. The ANOVA statistical tests were used to determine if a statistical difference between eolian and littoral samples could be detected based on traditional GSD metrics.

As grain microstructures can be related to grain-size (Vos et al. 2014), the sieving stage of the method involved sampling to determine the size class that best shows differences in grain shape as a function of MoT, described below. Also, a small range of grain-sizes resulted in easier filtering of imagery, also described below. Vos et al. (2014) suggest that a size class range from 3.25 φ to –1 φ is preferred for microtexture evaluation. The GSD of sediments from this study show that the 3 φ to 1.5 φ grain-size classes had sufficient grains for a representative statistical distribution (several hundred). Subsamples of several hundred grains were selected randomly using a spatula from each 1/4 φ sieve for each sample (including the cores) for use in the following analyses.

Subsampling and Structural Characterization

Subsamples were analyzed on a petri dish with an optical stereo microscope with 2–90× magnification and an attached digital camera with a resolution of 5 MP (Fig. 3A). Samples were magnified 20×; however, as long as a minimum pixel count of 200 per object is obtained (Kröner and

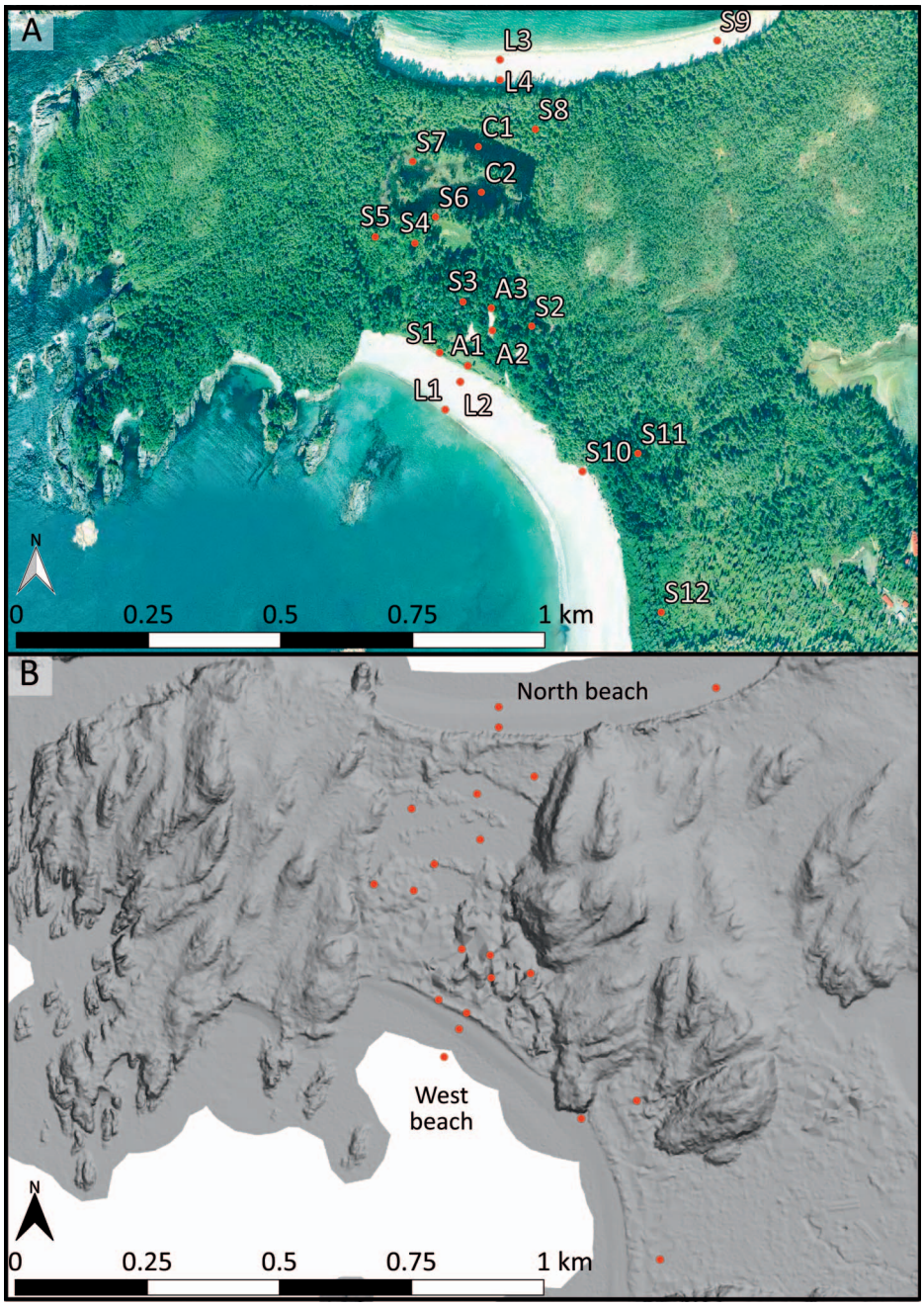

FIG. 2.—Locations of the samples used in this study. **A)** Digital orthophoto with sample labels. **B)** The hillshade lidar DEM from Figure 1 with beaches labeled.

Carbó 2013), other combinations of camera resolution and magnification are possible. The magnification had no bearing on results otherwise, as grain-size in the image is irrelevant in the analysis (only shape).

Images from each 1/4 φ size class were imported into the ImageJ shape-analysis software (Rasband 2010) (Fig. 3A). One method for deriving grain structure is provided in a downloadable macro plug-in for ImageJ (see Lewis et al. 2010). However, for this study, a simplified workflow was developed due to the bulk nature of the sediments, in contrast to Lewis et al. (2010), who examined thin sections prepared from cores. To convert the grain images to shapes required first thresholding images to black and white binary images (Fig. 3B). For the samples in this study, it was found that the Triangle thresholding method (Zack et al. 1977) utilizing the YUV color space (Y representing the luminance (brightness) component and UV representing the two chrominance (color) components) provided ideal thresholding for quartz grains. Next, thresholded binary images were measured for particle structure using the built-in ImageJ functionality (shape descriptor outputs described below). At this stage, particle size limits were specified as digital raster area limits per particle, and holes and edge effects (e.g., dark spots in the middle of grains causing a "hole" when the threshold was applied, and grains cut off at the edge of images) were eliminated.

As the particles were of a uniform size class, setting a narrow particle size limit reduced the amount of touching grains assigned to one particle (too large) as well as particulate matter that was difficult to threshold out (too small). This produced an image of particle outlines (Fig. 3C), each assigned unique numerical labels that were used for manual removal of anomalous or poorly digitized grains (Fig. 3D). The shape descriptors produced by the previous step in ImageJ include circularity, aspect ratio,

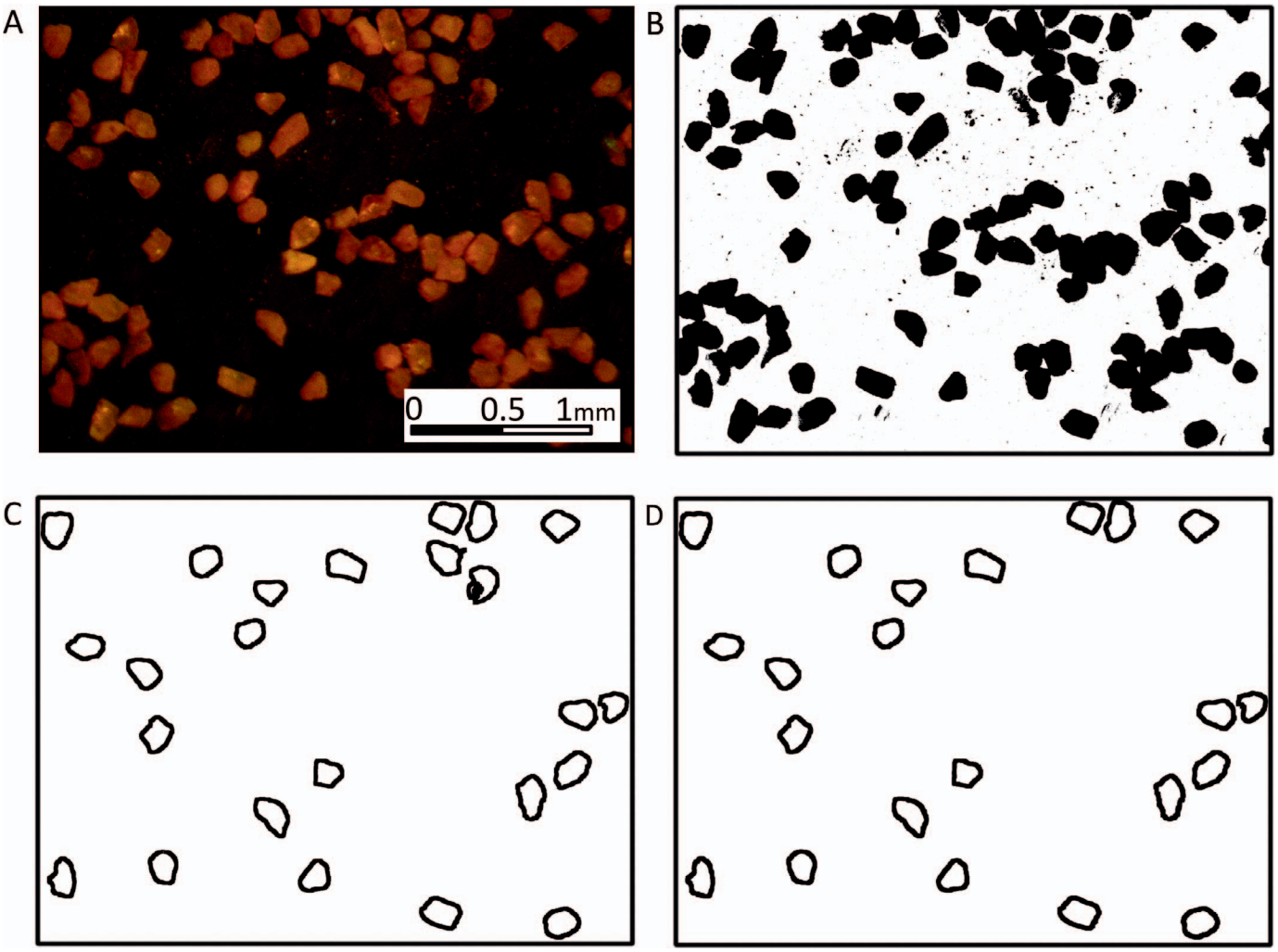

FIG. 3.—**A)** True color microphotograph of several dozen sand grains from a sample in the study area. **B)** Binary thresholded image of the same sample. **C)** Outline diagram of the same sample, with each particle that was not removed using the size threshold remaining. **D)** Manually edited image from which shape descriptors can be calculated.

roundness, and solidity. While these terms are familiar to sedimentologists, when applied to two-dimensional images they differ slightly from three-dimensional interpretations. Circularity is defined as

$$4\pi\left(\frac{Area}{[Perimeter]^2}\right) \tag{1}$$

and can range from zero to one, with one being a circle. This approximates sedimentological sphericity as described by Wadell (1932) and Krumbein (1941), but in two dimensions. Aspect ratio is simply

$$\frac{Major\ Axis}{Minor\ Axis} \tag{2}$$

and is a measure of elongation of the ellipse fitted to the particle as seen in two dimensions. Roundness is defined as

$$4\left(\frac{Area}{\pi[Major\ Axis]^2}\right) \tag{3}$$

which is similar to circularity in that a value of one would represent a circle. Roundness, however, measures area relative to a fitted ellipse, so it ignores irregular borders, and thus is different from the sedimentological definition of grain roundness as defined by Wadell (1932). The final measure is solidity, defined as

$$\frac{Area}{Convex\ area} \tag{4}$$

which measures the irregularity of the border, analogous to the sedimentological definition of roundness. Convex area, as calculated in this measure, can be described as the area of a polygon created around your shape with no interior angles greater than 180°, having the effect of all vertices of the polygon pointing away from the interior of the shape. These descriptors are illustrated in Figure 4.

Hypothesis Testing: Determination of Ideal Grain-Size and Shape

The process described above was repeated a minimum of five times for each 1/4 φ grain-size class of two calibration samples considered to be ideal representations of littoral and eolian environments (L1 (littoral) and A1 (eolian)) (Fig. 2). This was done to get a better distribution of shape descriptors, with a minimum of 100 grains sampled (Table 1). Generally, as grain-size decreased, number of grains sampled increased, as would be expected at a constant magnification. The results were aggregated for each

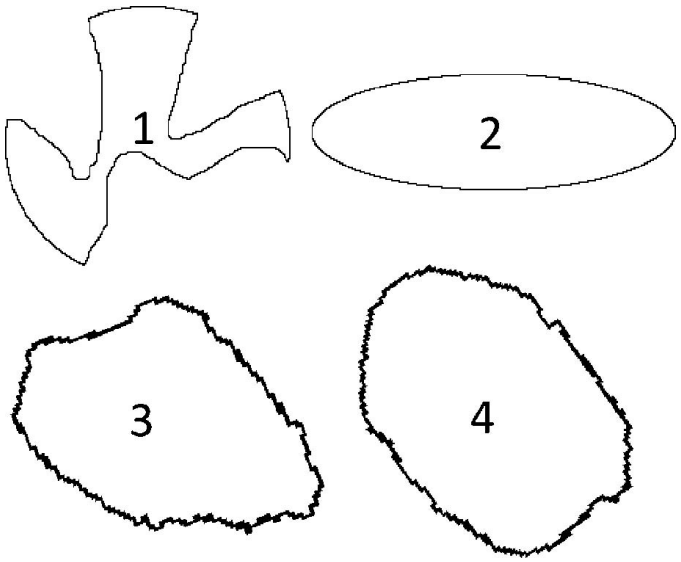

FIG. 4.—Exaggerated artificial "grains" (1 and 2), developed to illustrate the four shape descriptors calculated in ImageJ, and example grains from L1 (3) and A1 (4). Note that particle 1 is a circular grain with an irregular outer surface, and particle 2 is an elongate grain with a smooth outer surface. Shape descriptors for grains 1, 2, 3, and 4, respectively, are: circularity = (0.21, 0.58, 0.65, 0.73), aspect ratio = (1.50, 3.18, 1.52, 1.44), roundness = (0.67, 0.32, 0.66, 0.69), solidity = (0.53, 0.98, 0.92, 0.96).

size class, and the distributions were compared between the littoral and eolian sand using hypothesis testing (Table 1), where the null hypothesis is that the distribution of eolian and littoral sands are not statistically different, with the alternate hypothesis is that the distribution of eolian and littoral sands are statistically different.

First, an *F*-test of the equality of two variances was performed to compare the distributions (required for a valid *t*-test), with a *t*-test (*p*-value of 0.05) to determine if the distributions of shape descriptors are statistically different from each other, used to test the hypothesis. An ideal grain-size for this method can be defined as the grain-size class that shows, between a littoral and eolian sand, statistically different distributions of all shape descriptors, or as the grain-size that shows the strongest statistical difference in one (or more) shape descriptors. For this study, the former definition of ideal grain-size was used, and this was determined to be the 2.5 φ grain-size class (Table 1). Shape descriptors were then analyzed using the rest of the calibration samples (Table 2).

TABLE 2.—*Results of shape-parameter analysis for all calibration samples. n is the number of grains analyzed, μ is the mean, σ^2 is the variance. Note the consistently different mean and variance for the solidity variable between littoral and eolian samples.*

	$D = 2.5\varphi$					
		Circularity	Aspect Ratio	Roundness	Solidity	
	n	μ	μ	μ	μ	σ^2
A1	433	0.695	1.487	0.766	0.925	0.003
A2	267	0.686	1.363	0.755	0.929	0.009
A3	255	0.677	1.394	0.738	0.924	0.009
L1	351	0.665	1.476	0.708	0.913	0.012
L2	198	0.672	1.410	0.735	0.922	0.022
L3	203	0.677	1.373	0.748	0.912	0.013
L4	277	0.674	1.409	0.732	0.920	0.011

The samples listed in Table 2 expanded the calibration dataset and resulted in a greater range of littoral and eolian samples for comparison. In a broader-scale environmental reconstruction, this is akin to developing a full calibration dataset to compare to samples of unknown transport history. These data were also used to determine which shape parameters provide the best statistical separation of littoral and eolian sand. In this study, circularity and solidity are consistently different between littoral and eolian sands, and when hypothesis testing using difference of means is performed, solidity performed consistently better as a variable to differentiate littoral and eolian sediments with an 86% success rate of prediction. This is compared to 43% for circularity and 48% for aspect ratio and roundness (Table 3). The mean value for solidity was higher for eolian sands than for littoral sands (Table 2); however, it is conceded that the differences in mean values are within the reported variances. This was considered acceptable because the goal of this step of the method was to identify the ideal grain-size for differentiation. Of note, the higher average solidity values and lower variance in solidity values for eolian sediments is consistent with the concept of shape sorting via eolian processes preferentially entraining rounder grains (Mazzullo et al. 1986), as there is sufficient variance in solidity in the initial (littoral) grain population.

Hypothesis Testing: Remaining Samples

Following the determination of the ideal grain-size (2.5 φ) and shape descriptor (solidity), the distributions of solidity values from the ideal grain-size class from the calibration dataset were compared to samples of inferred MoT (S1 to S12, C1, and C3) to test the method. This involved

TABLE 1.—*Results of hypothesis testing for samples A1 and L1 for various grain diameters (D), with number of grains analyzed (n), decision (Y = statistically different, N = not statistically different) and t-test statistic in brackets. The mean solidity value for A1 and L1 are shown in the right-hand column.*

					Solidity	
D (φ)	n	Circularity	Aspect Ratio	Roundness	Different?	μ (A,L)
1.5	184	Y (6.17)	N (0.48)	N (1.45)	Y (2.86)	0.898,0.860
1.75	259	Y (4.89)	N (1.31)	Y (2.03)	Y (3.28)	0.898,0.863
2	706	Y (2.58)	N (1.79)	Y (2.29)	N (1.29)	0.881,0.872
2.25	531	Y (2.82)	N (0.54)	N (1.32)	N (1.76)	0.882,0.895
2.5	604	Y (5.78)	Y (3.34)	Y (3.31)	Y (5.15)	0.925,0.913
2.75	747	Y (5.18)	Y (2.53)	N (1.46)	Y (4.67)	0.920,0.901
3	818	Y (8.46)	N (0.61)	N (0.31)	Y (6.03)	0.921,0.901

TABLE 3.—*Results of hypothesis testing for the four shape descriptors calculated for the calibration samples, with decision (Y = statistically different, N = not statistically different) and t-test statistic in brackets. Note that the hypothetical case where all eolian sands are classified as statistically different from littoral sands would result in only Y within the outlined box and N outside of the box.*

Circularity	A1	A2	A3	L1	L2	L3	L4
A1							
A2	N (1.76)						
A3	N (1.29)	N (0.79)					
L1	Y (5.78)	Y (5.98)	Y (6.10)				
L2	N (0.64)	N (1.12)	N (0.47)	Y (3.41)			
L3	N (1.28)	N (0.68)	N (0.47)	Y (5.94)	N (0.52)		
L4	N (1.11)	N (1.06)	N (0.26)	Y (2.11)	N (0.27)	N (0.323)	
Aspect ratio	A1	A2	A3	L1	L2	L3	L4
A1							
A2	Y (2.63)						
A3	Y (3.57)	N (1.20)					
L1	Y (3.34)	Y (5.34)	Y (5.27)				
L2	Y (2.32)	N (1.43)	N (0.60)	Y (2.47)			
L3	Y (4.37)	N (0.38)	N (0.60)	Y (5.79)	N (1.34)		
L4	Y (3.02)	N (1.77)	N (0.65)	Y (4.92)	N (0.06)	N (1.57)	
Roundness	A1	A2	A3	L1	L2	L3	L4
A1							
A2	Y (2.51)						
A3	Y (2.94)	N (1.33)					
L1	Y (3.31)	Y (5.75)	Y (5.49)				
L2	N (1.31)	Y (2.43)	N (0.25)	Y (1.98)			
L3	Y (3.75)	N (0.52)	N (0.25)	Y (6.07)	N (1.07)		
L4	Y (2.46)	N (1.75)	N (0.53)	Y (3.14)	N (0.22)	N (1.44)	
Solidity	A1	A2	A3	L1	L2	L3	L4
A1							
A2	N (1.04)						
A3	N (1.04)	N (1.15)					
L1	Y (5.15)	Y (6.25)	Y (6.41)				
L2	N (1.61)	Y (1.98)	Y (2.85)	N (0.60)			
L3	Y (1.98)	Y (2.82)	N (1.84)	Y (5.67)	N (0.02)		
L4	Y (3.21)	Y (2.17)	Y (2.02)	N (1.52)	N (0.86)	N (0.99)	

obtaining subsamples of grains in the 2.5 φ size class of each sample, calculating the shape parameters from that subsample, and hypothesis testing to compare the distributions of solidity values from each sample against those of the calibration samples. Hypothesis testing was first conducted using the two calibration samples considered to be ideal representations of eolian and littoral environments (A1 and L1). If the sample was found to be statistically consistent with one of these calibration samples, the sample was assigned an MoT: eolian or littoral. If the sample was found to be statistically different from both calibration samples, then more tests were conducted using the remaining calibration samples (A2, A3, L2, L3, and L4).

RESULTS

Grain-Size Distributions

A graphic of the four GSD summary statistics are shown in Figure 5. The summary statistics of the GSD as well as the results of the one-way ANOVA tests are shown in Table 4.

TABLE 4.—*Grain-size summary statistics for samples analyzed in this study and results of one-way ANOVA statistical test. The hypothesis test is as follows: H_0: The two sample groups (eolian or littoral) are drawn from the same population; H_1: The two sample groups are drawn from different populations.*

MoT	Sample	D (φ)	Sorting (σ φ)	Skewness	Kurtosis
eolian	**A1**	2.372	0.327	0.063	Mesokurtic (0.965)
	A2	2.104	0.405	-0.035	Platykurtic (0.795)
	A3	2.059	0.376	-0.011	Platykurtic (0.877)
	S1	2.344	0.336	0.042	Mesokurtic (0.993)
	S2	2.230	0.337	0.081	Mesokurtic (1.086)
	S3	2.110	0.324	0.042	Mesokurtic (0.977)
	S4	2.767	0.401	0.019	Platykurtic (0.718)
	S5	2.149	0.549	-0.193	Leptokurtic (1.198)
	S6	2.338	0.344	0.027	Mesokurtic (1.017)
	S8	2.331	0.353	0.014	Mesokurtic (1.045)
	S11	2.091	0.323	0.034	Mesokurtic (1.095)
	S12	2.174	0.295	0.089	Mesokurtic (1.074)
littoral	**L1**	2.159	0.433	0.076	Mesokurtic (1.066)
	L2	2.541	0.477	-0.033	Mesokurtic (0.985)
	L3	2.269	0.325	-0.058	Leptokurtic (1.126)
	L4	1.894	0.403	-0.219	Leptokurtic (1.163)
	S9	2.200	0.317	0.184	Leptokurtic (1.189)
	S10	2.191	0.284	0.122	Mesokurtic (1.099)
Reject H_0?(p-value)		No (0.65)	No (0.80)	No (0.96)	No (0.06)

Figure 5 shows that basic grain-size summary statistics are not sufficient to elucidate transport mechanism. This is perhaps due to a fairly wide spread in the mean grain-size and sorting of the eolian sediments, which can be largely attributed to two dune sediment samples from the western portion of the study area. One sample (S5) was poorly sorted when compared to other samples, and another (S4) was finer than other samples. Even if those are treated as outliers, however, MoT differentiation is difficult. In addition, skewness, which can be diagnostic in eolian or beach environments (Mason and Folk 1958), did not clearly distinguish between these environments here (Fig. 5). Generally, the only observable difference in Figure 5 is the generally higher kurtosis values for littoral samples, but it is hardly diagnostic. This is reflected in the one-way ANOVA tests, where the only test that yielded a *p*-value at all close to the cutoff α of 0.05 was between the distribution of eolian and littoral kurtosis values (Table 4); however they were still found to be drawn from the same statistical distribution (i.e., kurtosis could not be used with these samples to statistically differentiate eolian and littoral sediments).

Using the Ideal Grain-Size and Solidity Shape Descriptor to Predict MoT

When the solidity shape descriptor was calculated for the other samples (S2 to S9, S11, S12, C1, and C3), it could be used to predict the MoT as inferred from ancillary data or the modern landform (S1, S10) 76% of the time (Table 5). The method performed well on littoral sediments, correctly identifying all of them. The eolian sand samples that were not statistically differentiated from beach sands (S2, S4, S12, and C03-20) all could be identified as eolian samples if the statistical threshold was lowered. The most similar calibration sample (corresponding to the lowest *t*-test statistic) for each sample was A1, the modern foredune sample. Lowering the statistical threshold, however, would increase the likelihood of Type 1 error. A plot of the mean solidity values and the variance in the distribution of the values shows that solidity is higher in eolian samples and, generally, variance in eolian solidity values is lower (Fig. 6). This plot contrasts with Figure 5, where there was no clear difference in the GSD summary statistics between eolian and littoral samples, and could reflect a difference in the variables involved in the physical processes of sediment transport (mineralogy, roundness, fluid flow competency, and beach fetch) that are discussed below.

DISCUSSION

Effectiveness of the Method

This paper documents a new, efficient method for differentiating sediments transported via eolian or littoral processes that requires only inexpensive equipment and free software. It requires a relatively small sample size to produce a statistically robust distribution of sand-grain shape parameters. In practice, this method could, with additional pre-processing to remove cementation, be applied to consolidated sands or sediments that have undergone partial or complete diagenesis. When GSD

TABLE 5.—*Results of hypothesis testing for samples with the number of sand grains (n), MoT as interpreted from ancillary data, and decision (Y = statistically different, N = not statistically different) with the* t*-test statistic in brackets. If the "not statistically different" decision (N) at the 95% confidence level corresponded with the MoT as inferred from ancillary data (eolian or littoral), then the method was labeled correct (Yes).*

	n	MoT	A1	A2	A3	L1	L2	L3	L4	Correct?
S1	247	Eolian	N (0.65)			Y (4.03)				Yes
S2	259	Eolian	Y (2.76)	Y (2.90)	Y (2.09)	Y (5.47)	Y (3.62)	Y (4.98)	Y (3.01)	No
S3	237	Eolian	Y (3.33)	Y (2.04)	N (0.91)	Y (4.48)				Yes
S4	298	Eolian	Y (3.63)	Y (3.45)	Y (4.36)	Y (5.11)	Y (4.69)	Y (4.91)	Y (3.84)	No
S5	191	Eolian	Y (2.91)	N (1.49)	Y (2.19)	Y (4.30)				Yes
S6	223	Eolian	N (0.54)			Y (2.74)				Yes
S7	310	Eolian	N (1.88)			Y (2.22)				Yes
S8	288	Eolian	Y (2.13)	N (1.61)	Y (3.67)	Y (5.83)				Yes
S11	250	Eolian	N (1.29)			Y (3.81)				Yes
S12	314	Eolian	N (0.44)	Y (2.54)	Y (3.34)	N (1.45)	N (1.57)	N (0.95)	Y (2.34)	No
C01-49	224	Eolian	N (0.80)			Y (5.59)				Yes
C03-20	207	Eolian	Y (2.32)	Y (2.79)	Y (3.19)	Y (4.99)	Y (3.90)	Y (4.74)	Y (3.82)	No
S9	204	Littoral	Y (4.59)			N (1.10)				Yes
S10	321	Littoral	Y (3.35)			N (1.73)				Yes
C01-62	213	Littoral	Y (4.47)			Y (2.59)	N (0.89)	Y (2.95)	Y (2.00)	Yes
C01-95	189	Littoral	Y (5.43)			Y (2.46)	N (1.44)	N (1.83)	Y (2.10)	Yes
C03-40	145	Littoral	Y (4.19)			Y (2.02)	Y (2.55)	N (1.06)	Y (2.46)	Yes

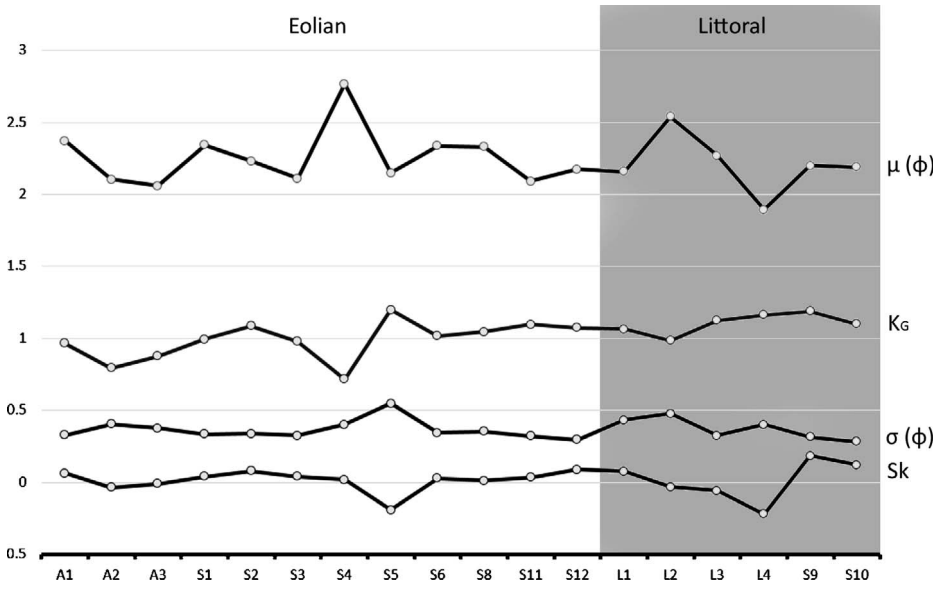

FIG. 5.—Plot of GSD summary statistics: mean (μ) and standard deviation (σ) in phi, kurtosis (Kg), and skewness (Sk). Littoral samples are plotted in the shaded area for clarity.

analyses fail to yield any diagnostic traits from which distinct mechanisms of transport can be discerned (e.g., Table 4, Figs. 5, 6), or when they need additional evidence to support findings, this method can be used to provide additional diagnostic results to aid in interpretations of mechanisms of transport (MoT) and help with broader landscape interpretation and/or reconstruction. The method is nondestructive, and the grain population used can be recombined with the original sample. The small sample size allows researchers to apply the method to sediments obtained using a range of sample collection methods, such as cores, grab samples, or augers. While it was found that solidity was the shape parameter most useful for differentiating littoral and eolian sediment in this study, the variety of shape parameters calculated by ImageJ may assist in extending the method to different MoT or regional settings where other parameters may be more significant in detecting differences.

Decoupling of distinct grain solidity classes occurred over relatively short distances in this study, but decoupling of distinct grain-size classes did not (cf. Bauer 1991). This may be attributable to the different physical processes acting on the grain that initiate transport. Decoupling of sediments into different grain-size classes depends largely on the specific shear stress acting on the bed overcoming the gravitational force provided by grains of different mass; larger, heavier grains provide a greater resistance than smaller, lighter grains. Shape sorting, however, results from a change in the internal angle of friction and the amount of packing, where well rounded grains will have fewer contact points (lower internal friction) and are less likely to pack tightly, thereby reducing the magnitude of shear stress required to initiate transport. There may be certain combinations of mineralogy, roundness, fluid flow competency, and beach fetch that yield conditions right for shape sorting and others for size sorting, although this was not discernible in this study.

When the calibrated method was applied to samples for which there were ancillary data to support a MoT, or to samples collected from a modern landform, it provided corroborating evidence of the MoT for 76% of the samples. Of the remaining samples, statistically ambiguous results (i.e., results that did not identify a MoT with 95% confidence) still yielded information leading toward the likely MoT through the lowest test statistic and, thus, the calibration sample most similar to the test sample. The eolian samples whose MoT was successfully identified in Table 5 show that the results might be used for discriminating the type of eolian or littoral depositional setting. For example, S6, S7, S11, and C01-49 were all identified as being most similar to calibration sample A1, which was

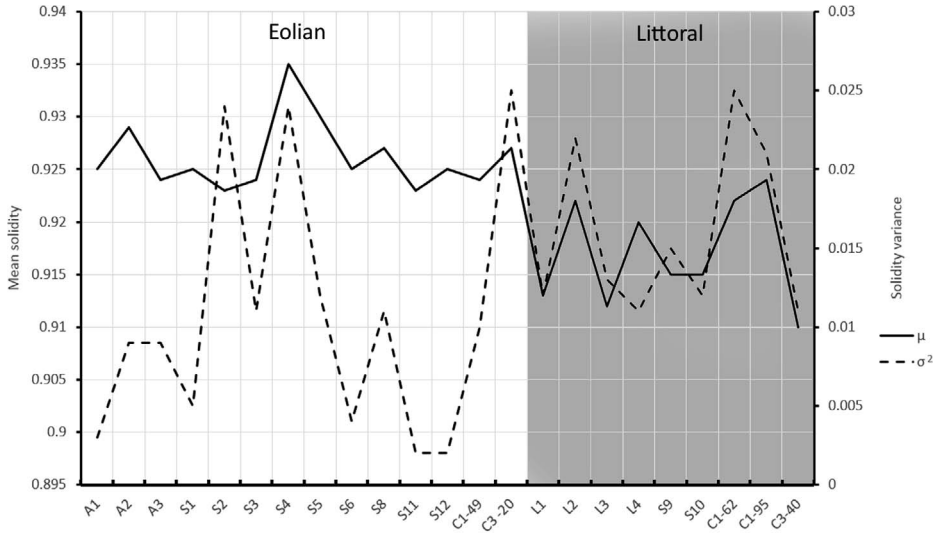

FIG. 6.—Plot of mean solidity values (μ) and the variance in the distribution of solidity values (σ^2) for each sample. Littoral samples are plotted in the shaded area for clarity. Note the lower mean solidity values and generally higher variance found in littoral samples.

collected from the modern foredune. The interpretation that these samples represent sediments deposited in a foredune agrees with ancillary data, which suggest that these sands are part of a foredune complex. Two samples (S5 and S8) were identified as having sediments derived from a MoT most similar to the calibration sample from the deflation basin of a blowout dune (A2). The bare-earth DEM (Fig. 2) shows that both samples were collected in low-relief, topographically flat regions and, thus, are unlikely to be part of a foredune ridge (A1) or a depositional lobe (A3). Finally, sample S3 was determined to be most similar to calibration sample A3, and it appears in the lee of a large, ~ 15 m-tall, blowout depositional lobe. Thus, the most likely MoT for sample S3 is by wind in the area of flow separation and grain fallout behind a dune in an environment similar to a depositional lobe.

Limitations of the Methodology and Future Work

The method presented can be modified in future studies to broaden its application or to further investigate sediment transport processes and related depositional settings. In landscapes with a more complex geomorphic history (e.g., an embayed beach with appreciable fluvial inputs), a calibration dataset that includes more, or different, MoTs might be used to differentiate a broader suite of landforms or strata (e.g., fluvial, glaciofluvial, lacustrine, or marine). Also, mineralogical separation to isolate quartz or different opacities of quartz could be useful for improving the method or expanding it to different MoTs (cf. Gomez et al. 1988). In this study, grains were separated for mineralogy through the digital thresholding process (Fig. 3B); darker grains such as micas and opaque feldspars were removed by the triangle thresholding method based on the YUV color space. A basic assumption of this approach is that, by thresholding out darker grains, the remaining mineralogy of the sample is largely homogeneous (in this case, composed mostly of quartz). Thresholding techniques might be further facilitated by using sediment that consists of minerals with distinct colors or opacities. For example, the thresholding technique could be used to remove light-colored (quartz) grains to isolate and examine only feldspars or heavy (e.g., magnetite) grains. Future work could also investigate regional sediment transport histories that influence particle shape. It is possible that the transport histories of the samples presented here are more complex than littoral transport to the backshore followed by eolian transport over the beach and into dune deposits.

In addition, the geological setting and resulting sedimentological properties of the study area may partly control shape sorting or grain rounding. For instance, the northwestern portion of Calvert Island consists mainly of coarse-grained granodiorite (Roddick 1996) that erodes readily under current climatic conditions. Weather stations installed on the island give annual temperature averages of between 9 and 10 degrees Celsius and mean annual precipitation of 3000 to 3500 mm, conditions that are conducive to extensive bedrock weathering. This weathering produces regolith and sand-size "young" sediments with subangular grains that can be modified over relatively short distances by wind or water. The recently stabilized landforms on Calvert Island's northwestern coast preserve these young sediments (Neudorf et al. 2015b), which still contain appreciable amounts of feldspar that has yet to disintegrate into clays.

These sedimentological properties are in contrast to those in other coastal regions that contain more mature sediments, or sediments that are much less resistant to weathering. For example, minor glaciation in Australia (both spatially and temporally) through the Pleistocene (Barrows et al. 2001) resulted in the development of very mature sands consisting of well rounded, mostly quartz grains. It is possible that in that environment the method presented here could be unsuccessful, as subtle differences in well-rounded quartz grains would be difficult to resolve in two-dimensional imagery. In Hawaii, coastal sediments are typically dominated by calcareous sands eroded from fringing reefs, with minor fractions of mafic volcanic minerals (Fletcher et al. 2011). These sands, which are highly susceptible to weathering and dissolution, are much softer than quartz and feldspar, and thus the window for shape sorting that generates appreciable differences in grain rounding may be too small to detect using our method.

CONCLUSIONS

The aim of this study was to develop a method that requires inexpensive and easily obtainable equipment and software that differentiates littoral and eolian sediments to aid in landscape interpretation and environmental reconstruction using sands stored in relict landforms. The method is based on the principle of shape sorting due to eolian transport (Mazzullo et al. 1986). It was found that solidity, akin to sedimentological roundness, most commonly (86% of the time) showed a statistical difference between littoral and eolian sands. The method performed well, predicting the MoT of sands of relict landforms 76% of the time. Avenues for further investigation of this method include testing in different geomorphic, mineralogic, and climatic environments, extension to different MoTs, and performing basic mineralogical separation beforehand. Opportunities for integration of these data with other diagnostic sand-grain data (such as petrology, electron microscopy, or GSD) exist. Some evidence suggests that our method may also predict subenvironments (such as upper beach, lower beach, foredune crest, or depositional lobe) from calibration samples.

ACKNOWLEDGMENTS

This research was generously and primarily supported financially and logistically by partners at the Hakai Institute and Tula Foundation, notably Eric Peterson and Christina Munck. This project was also funded by a National Science and Engineering Research Council Postgraduate Scholarship to JBRE, a Mitacs Elevate Postdoctoral Fellowship to DHS, a Hakai Postdoctoral Fellowship to CMN, and NSERC Discovery grants to IJW and OBL. The authors are grateful for field assistance provided by Alex Lausanne, Libby Griffin, Jordan Bryce, Daniel Huesken, and Brie Mackovic. The authors recognize that this study took place on the traditional territory of the Heiltsuk and Wuikinuxv First Nations, and are grateful for the opportunity.

REFERENCES

Anderson, R.S., Sørensen, M., and Willets, B.B., 1991, A review of recent progress in our understanding of aeolian sediment transport: Aeolian Grain Transport, Vienna, Springer, v. 1, p. 1–19,

Barrows, T.T., Stone, J.O., Fifield, L.K., and Cresswell, R.G., 2001, Late Pleistocene glaciation of the Kosciuszko Massif, Snowy Mountains, Australia: Quaternary Research, v. 55, p. 179–189.

Bauer, B.O., 1991, Aeolian decoupling of beach sediments: Association of American Geographers Annual, v. 81, p. 290–303.

Bendle, J.M., Palmer, A.P., and Carr, S.J., 2015, A comparison of micro-CT and thin section analysis of late Glacial glaciolacustrine varves from Glen Roy, Scotland: Quaternary Science Reviews, v. 114, p. 61–77.

Blott, S.J., and Pye, K., 2001, GRADISTAT: a grain size distribution and statistics package for the analysis of unconsolidated sediments: Earth Surface Processes and Landforms, v. 26, p. 1237–1248.

Clague, J.J., 1976, Quadra Sand and its relation to the late Wisconsin glaciation of southwest British Columbia: Canadian Journal of Earth Sciences, v. 13, p. 803–815.

Culver, S.J., Bull, P.A., Campbell, S., Shakesby, R.A., 1983, Environmental discrimination based on quartz grain surface textures: a statistical investigation: Sedimentology, v. 30, p. 129–136.

Fletcher, C.H., Romine, B.M., Genz, A.S., Barbee, M.M., Dyer, M., Anderson, T.R., Lim, S.C., Vitousek, S., Bochicchio, C., and Richmond, B.M., 2011, National assessment of shoreline change: historical shoreline change in the Hawaiian Islands: U.S. Geological Survey, Open-File Report 2011-1051, 55 p.

Folk, R.L., 1966, A review of grain size parameters: Sedimentology, v. 6, p. 73–93.

Folk, R.L., and Ward, W.C., 1957, Brazos River bar: a study in the significance of grain size parameters: Journal of Sedimentary Petrology, v. 27, p. 3–26.

Fournier, G.R., 1964, Partial immersion technique for the photography of sand grain surfaces: Journal of Sedimentary Petrology, v. 34, p. 473–482.

Friedman, G.M., 1961, Distinction between dune, beach, and river sands from their textural characteristics: Journal of Sedimentary Petrology, v. 31, p. 514–529.

Gomez, B., Dowdeswell, J.A., and Sharp, M., 1988, Microstructural control of quartz sand grain shape and texture: implications for the discrimination of debris transport pathways through glaciers: Sedimentary Geology, v. 57, p. 119–129.

Houser, C., 2009, Synchronization of transport and supply in beach-dune interaction: Progress in Physical Geography, v. 33, p. 733–746.

Kasper-Zubillaga, J.J., 2009, Roundness in quartz grains from inland and coastal dune sands, Altar Desert, Sonora, Mexico: Sociedad Geológica Mexicana, Boletín, v. 61, p. 1–12.

Kasper-Zubillaga, J.J., and Dickinson, W.W., 2001, Discriminating depositional environments of sands from modern source terranes using modal analysis: Sedimentary Geology, v. 143, p. 149–167.

Kasper-Zubillaga, J.J., Dickinson, W.W., Carranza-Edwards, A., and Hornelas-Orozco, Y., 2005, Petrography of quartz grains in beach and dune sands of Northland, North Island, New Zealand: New Zealand Journal of Geology and Geophysics, v. 48, p. 649–660.

Krinsley, D.H., and Donahue, J., 1968, Environmental interpretation of sand grain surface textures by electron microscopy: Geological Society of America, Bulletin, v. 79, p. 743–748.

Kröner, S., and Carbó, M.T.D., 2013, Determination of minimum pixel resolution for shape analysis: proposal of a new data validation method for computerized images: Powder Technology, v. 245, p. 297–313.

Krumbein, W.C., 1941, Measurement and geological significance of shape and roundness of sedimentary particles: Journal of Sedimentary Research, v. 11, p. 64–72.

Lewis, T., Francus, P., Bradley, R.S., and Kanumaru, K., 2010, An automated system for the statistical analysis of sediment texture and structure at the micro scale: Computers & Geosciences, v. 36, p. 1374–1383.

Mason, C.C., and Folk, R.L., 1958, Differentiation of beach, dune, and eolian flat environments by size analysis, Mustang Island, Texas: Journal of Sedimentary Petrology, v. 28, p. 211–226.

Mazzullo, J., Sims, D., and Cunningham, D., 1986, The effects of eolian sorting and abrasion upon the shapes of fine quartz sand grains: Journal of Sedimentary Petrology, v. 56, p. 45–56.

McLaren, D., Fedje, D., Hay, M., Mackie, Q., Walker, I.J., Shugar, D.H., Eamer, J.B.R., Lian, O.B., and Neudorf, C., 2014, A post-glacial sea-level hinge on the central Pacific coast of Canada: Quaternary Science Reviews, v. 97, p. 148–169.

Moss, A.J., and Green, P., 1975, Sand and silt grains: Predetermination of their formation and properties by microfractures in quartz: Geological Society of Australia, Journal, v. 22, p. 485–495.

Neudorf, C.M., Brennand, T.A., and Lian, O.B., 2015a, Comparisons between macro- and microfabrics in a pebble-rich, sandy till deposited by the Cordilleran Ice Sheet: Boreas, v. 44, p. 483–501.

Neudorf, C.M., Lian, O.B., Walker, I.J., Shugar, D.H., Eamer, J.B.R., and Griffen, L.C.M., 2015b, Toward a luminescence chronology for coastal dune and beach deposits on Calvert Island, British Columbia central coast, Canada: Quaternary Geochronology, v. 30, p. 275–281.

Potter, P.E., 1986, South America and a few grains of sand: part 1, beach sands: Journal of Geology, v. 94, p. 301–319.

Purkait, B., 2010, The use of grain-size distribution patterns to elucidate aeolian processes on a transverse dune of Thar Desert, India: Earth Surface Processes and Landforms, v. 35, p. 525–530.

Purkait, B., and Majumdar, D.D., 2014, Distinguishing different sedimentary facies in a deltaic system: Sedimentary Geology, v. 308, p. 53–62.

Rasband, W.S., 2010, ImageJ, U.S. National Institute of Health, Bethesda, Maryland, USA: http://rsb.info.nih.gov/ij/docs/index.html.

Roddick, J.A., 1996, Geology, Rivers Inlet–Queens Sound, British Columbia (92M), (102P): Geological Survey of Canada, Open File 3278.

Rogerson, R.J., and Hudson, H.M., 1983, Quartz surface microtextures and grain-size characteristics of Quaternary sediments in the Porcupine Strand area of coastal Labrador, Newfoundland, Canada: Canadian Journal of Earth Sciences, v. 20, p. 377–387.

Shennan, I., Bradley, S., Milne, G., Brooks, A., Bassett, S., and Hamilton, S., 2006, Relative sea-level changes, glacio isostatic modelling and ice-sheet reconstructions from the British Isles since the Last Glacial Maximum: Journal of Quaternary Science, v. 21, p. 585–599.

Shugar, D.H., and Clague, J.J., 2011, The sedimentology and geomorphology of rock avalanches on glaciers: Sedimentology, v. 58, p. 1762–1783.

Shugar, D.H., Walker, I.J., Lian, O.B., Eamer, J.B.R., Neudorf, C., McLaren, D., and Fedje, D., 2014, Post-glacial sea-level change along the Pacific coast of North America: Quaternary Science Reviews, v. 97, p. 170–192.

Soutendam, C.J.A., 1967, Some methods to study surface textures of sand grains: Sedimentology, v. 8, p. 281–290.

Stark, N., Hay, A.E., Chee, R., and Lake, C.B., 2014, The impact of particle shape on the angle of internal friction and the implications for sediment dynamics at a steep, mixed sand–gravel beach: Earth Surface Dynamics, v. 2, p. 469–480.

Sun, D., Bloemendal, J., Rea, D.K., Vandenberghe, J., Jiang, F., An, Z., and Su, R., 2002, Grain-size distribution function of polymodal sediments in hydraulic and aeolian environments, and numerical partitioning of the sedimentary components: Sedimentary Geology, v. 152, p. 263–277.

Van Der Meer, J.J.M., and Menzies, J., 2011, The micromorphology of unconsolidated sediments: Sedimentary Geology, v. 238, p. 213–232.

Vincent, P., 1986, Differentiation of modern beach and coastal dune sands: a logistic regression approach using the parameters of the hyperbolic function: Sedimentary Geology, v. 49, p. 167–176.

Vos, K., Vandenberghe, N., and Elsen, J., 2014, Surface textural analysis of quartz grains by scanning electron microscopy (SEM): from sample preparation to environmental interpretation: Earth-Science Reviews, v. 128, p. 93–104.

Wadell, H., 1932, Volume, shape, and roundness of rock particles: The Journal of Geology, v. 40, p. 443–451.

Warnke, D.A., and Gram, R., 1969, The study of mineral-grain surfaces by interference microscopy: Notes: Journal of Sedimentary Petrology, v. 39, p. 1599–1604.

Zack, G.W., Rogers, W.E., and Latt, S.A., 1977, Automatic measurement of sister chromatid exchange frequency: The Journal of Histochemistry and Cytochemistry, v. 25, p. 741–753.

Received 29 June 2016; accepted 8 November 2016.